

Growth dynamics of reactive-sputtering-deposited AlN films

M. A. Auger, L. Vázquez, O. Sánchez, M. Jergel, R. Cuerno et al.

Citation: *J. Appl. Phys.* **97**, 123528 (2005); doi: 10.1063/1.1937467

View online: <http://dx.doi.org/10.1063/1.1937467>

View Table of Contents: <http://jap.aip.org/resource/1/JAPIAU/v97/i12>

Published by the [American Institute of Physics](#).

Additional information on *J. Appl. Phys.*

Journal Homepage: <http://jap.aip.org/>

Journal Information: http://jap.aip.org/about/about_the_journal

Top downloads: http://jap.aip.org/features/most_downloaded

Information for Authors: <http://jap.aip.org/authors>

ADVERTISEMENT



AIPAdvances

Now Indexed in
Thomson Reuters
Databases

Explore AIP's open access journal:

- Rapid publication
- Article-level metrics
- Post-publication rating and commenting

Growth dynamics of reactive-sputtering-deposited AlN films

M. A. Auger,^{a)} L. Vázquez, and O. Sánchez

*Instituto de Ciencia de Materiales de Madrid–Consejo Superior de Investigaciones Científicas (CSIC),
C/Sor Juana Inés de la Cruz 3, E-28049, Cantoblanco, Madrid, Spain*

M. Jergel

*Institute of Physics, Slovak Academy of Sciences, Dubravská cesta 9, 845 11 Bratislava 45,
Slovak Republic*

R. Cuerno

*Departamento de Matemáticas and Grupo Interdisciplinar de Sistemas Complejos, Universidad Carlos III
de Madrid, Avenida de la Universidad 30, E-28911, Leganés, Madrid, Spain*

M. Castro

*Grupo Interdisciplinar de Sistemas Complejos and Grupo de Dinámica No Lineal, Escuela Técnica
Superior de Ingeniería (ICAI), Universidad Pontificia Comillas, E-28015, Madrid, Spain*

(Received 4 January 2005; accepted 28 April 2005; published online 23 June 2005)

We have studied the surface kinetic roughening of AlN films grown on Si(100) substrates by dc reactive sputtering within the framework of the dynamic scaling theory. Films deposited under the same experimental conditions for different growth times were analyzed by atomic force microscopy and x-ray diffraction. The AlN films display a (002) preferred orientation. We have found two growth regimes with a crossover time of 36 min. In the first regime, the growth dynamics is unstable and the films present two types of textured domains, well textured and randomly oriented, respectively. In contrast, in the second regime the films are homogeneous and well textured, leading to a relative stabilization of the surface roughness characterized by a growth exponent $\beta = 0.37 \pm 0.03$. In this regime a superrough scaling behavior is found with the following exponents: (i) Global exponents: roughness exponent $\alpha = 1.2 \pm 0.2$ and $\beta = 0.37 \pm 0.03$ and coarsening exponent $1/z = 0.32 \pm 0.05$; (ii) local exponents: $\alpha_{loc} = 1$, $\beta_{loc} = 0.32 \pm 0.01$. The differences between the growth modes are found to be related to the different main growth mechanisms dominating their growth dynamics: sticking anisotropy and shadowing, respectively. © 2005 American Institute of Physics. [DOI: 10.1063/1.1937467]

I. INTRODUCTION

The study of kinetic surface roughening under far-from-equilibrium conditions has attracted the interest of researchers in recent years.^{1–4} In spite of its complexity, many studies, both theoretical and experimental, have proven the existence of kinetic surface roughening in growth processes. These findings have practical importance in thin-film growth because kinetic roughening is related to the spatial and temporal correlations of surface roughness as growth proceeds. This kind of study is especially relevant when different scaling laws displayed by the kinetic roughening can be related to specific growth mechanisms.⁵ The characterization of surface film growth at the submicron level as well as knowledge of the mechanisms governing the film morphology may be very useful for future applications in fields related to nanotechnology. Thus, it becomes very important to apply these studies to films of technological interest, which are usually grown under far-from-equilibrium conditions. This is the case of aluminum nitride (AlN) films grown by dc reactive magnetron sputtering, which present excellent electronic, mechanical, and chemical properties. These special charac-

teristics make AlN coatings very promising for use as protective coatings,^{6,7} elements in electronic devices⁸ (due to the wide band gap of 6.2 eV of AlN), selective detectors,⁹ etc. In particular, the use of AlN films as buffer layers has promising features for the fabrication of optoelectronic devices as photodetectors, light-emitting diodes, laser diodes, etc.¹⁰ For instance, GaN epilayers are typically used in these devices. Here, the inclusion of an AlN buffer layer with the adequate thickness leads to a superior crystal quality and a better optical performance of the GaN epilayer.¹¹ Recently, it has been reported that both the grain size and nuclei density of the AlN buffer layer play a key role in the quality of the GaN epilayer.¹² Besides, aluminum nitride is known to be one of the most promising piezoelectric materials for high-frequency surface acoustic wave (SAW) devices¹³ because of its high sound velocity. To obtain proper SAW devices, the corresponding film must have not only a high electrical resistivity and good piezoelectric properties, but also a low surface roughness. Thus, a detailed surface morphology characterization is needed in this case. Due to its wide range of applications, in the previous years a great number of publications has been devoted to studying the structural, optical, or mechanical characteristics of AlN coatings.^{14,15} Although there are some publications dealing with the dynamic scaling growth of materials deposited by sputtering techniques,^{16–19}

^{a)}Present address: Centro Nacional de Investigaciones Metalúrgicas (CENIM-CSIC) Avda. Gregorio del Amo, 8. 28040 Madrid, Spain; electronic mail: maauger@icmm.csic.es

to our knowledge, there is none devoted to the study of AIN film growth. In many of these systems, the studies of sputter-deposited films give different results (i.e., larger exponent values) than those predicted by the existing growth models.^{17–19} A clear explanation of this fact is lacking. Thus, our aim is to obtain a deeper insight of the growing mechanisms governing the surface morphology of this material by means of a detailed characterization of the evolution of the film surface morphology under the framework of dynamic scaling theory.^{2,3}

This theory has proven to be very useful for the study of surface growth because it allows the knowledge of the main physical mechanisms governing the film surface growth. Thus, it has been applied to study the dynamics of surface growth for films produced by evaporation, sputtering, chemical vapor deposition, sedimentation, electrodeposition, chemical and ion-beam etching, etc.^{2,3} However, despite the evident success of this theory, its correspondence with some experimental systems is still incomplete. This deficiency can be due, among other reasons, to the lack of models for two-dimensional substrates, which allow for a more direct comparison with the film-growth experimental data, and the complexity of the growth systems. However, the effort to address the understanding of these complex systems is worthy because many films with technological applications are deposited in such conditions.

The statistical properties of a rough surface can be characterized by the fluctuations of the surface height $h(\vec{r}, t)$, around its mean value $\langle h \rangle$, namely, through the interface width defined as $w(r, t) = \langle (h(\vec{r}, t) - \langle h \rangle)^2 \rangle_r^{1/2}$, where t is the deposition time and $\langle \dots \rangle_r$ denotes the average over all \vec{r} in a system of size L and $r \leq L$. Two important quantities are derived from this general expression. The first one is the global width or root-mean-square roughness $\sigma(L, t) = w(L, t)$ corresponding to the case $r = L$, and the second one is the local width $w(r, t)$, where $r \leq L$. In the standard dynamical scaling theory, both the global and local widths follow the Family–Vicsek (FV) dynamic scaling as²⁰

$$w(r, t) = t^{\alpha/z} f(r/t^{1/z}), \quad (1)$$

where the scaling function $f(u)$ behaves as

$$f(u) \propto \begin{cases} u^\alpha & \text{if } u \ll 1, \\ \text{const} & \text{if } u \gg 1. \end{cases} \quad (2)$$

In this case, the roughness exponent α and the dynamic exponent z characterize the universality class of the model under study. The ratio $\beta = \alpha/z$ is the growth exponent describing the surface roughening process in time through the power-law behavior $\sigma \propto t^\beta$. The roughness exponent describes the lateral correlations of the surface roughness, and $1/z$ is known as the coarsening exponent describing the coarsening process of the typical lateral correlation length of the system, ξ , which is usually related to the grain size. Although many systems have been found to follow FV scaling,^{2,3} numerical studies and models, as well as experimental observations, have identified the existence of the so-called anomalous scaling.²¹ This anomalous roughening is characterized by a different scaling for global and local sur-

face fluctuations. This leads to the existence of a set of independent, local roughness and growth exponents, α_{loc} and β_{loc} , respectively, which characterizes the local interface fluctuations on the scales $r \ll L$. These local exponents differ from the global ones, α and β . In particular, in these anomalous systems the local width obeys the following scaling relationship:

$$w(r, t) = t^{\alpha/z} f_A(r/t^{1/z}), \quad (3)$$

where the scaling function $f_A(u)$ behaves as

$$f_A(u) \propto \begin{cases} u^{\alpha_{\text{loc}}} & \text{if } u \ll 1, \\ \text{const} & \text{if } u \gg 1. \end{cases} \quad (4)$$

The scaling properties of the local surface fluctuations can be investigated by different means. One possibility is to characterize and compute directly the global and local interface widths.²² Other analyses rely on the study and computation of different functions that describe statistically the surface morphology. One of these functions is the square root of the height-difference correlation function, $G_2(r, t) = \{ \langle [h(\vec{r}' + \vec{r}, t) - h(\vec{r}', t)]^2 \rangle \}^{1/2}$, which scales as $w(r, t)$.^{2,3} The other function is the structure factor or power spectral density (PSD) defined as $\text{PSD}(k, t) = \langle H(k, t)H(-k, t) \rangle$, where $H(k, t)$ is the Fourier transform of the surface height in a system of lateral size L , k being the spatial frequency in the reciprocal space. It can be seen²³ that, for an anomalous $2+1$ -dimensional system, the PSD function follows the scaling relationship

$$\text{PSD}(k, t) = k^{-(2\alpha+2)} f_P(kt^{1/z}), \quad (5)$$

where

$$f_P(p) \propto \begin{cases} p^{2\alpha+2} & \text{if } p \ll 1, \\ p^{2(\alpha-\alpha_s)} & \text{if } p \gg 1, \end{cases} \quad (6)$$

α_s being known as the spectral roughness exponent.²⁴

From the different sets of α , α_{loc} , and α_s values, up to four scaling behaviors are expected.²³ Three of them have already been observed experimentally,⁴ namely,

- (i) FV standard scaling, which occurs when $\alpha = \alpha_{\text{loc}} = \alpha_s < 1$;
- (ii) Intrinsic anomalous scaling, which takes place when $\alpha \neq \alpha_{\text{loc}} = \alpha_s < 1$; and
- (iii) Superrough scaling for $1 = \alpha_{\text{loc}} \neq \alpha = \alpha_s > 1$.

In this work we will focus our attention on the third case, which is present in our system. In this case, the function $G_2(r, t)$ follows the form^{23,25}

$$G_2(r, t)/r^\alpha \propto \begin{cases} (r/t^{1/z})^{-(\alpha-\alpha_{\text{loc}})} & \text{if } r/t^{1/z} \ll 1, \\ (r/t^{1/z})^{-\alpha} & \text{if } r/t^{1/z} \gg 1, \end{cases} \quad (7)$$

where we have substituted ξ for $t^{1/z}$.¹⁹ From this behavior, it is evident that the $G_2(r, t)$ curves obtained for different times do not overlap for small r values since $\alpha - \alpha_{\text{loc}} \neq 0$, i.e., the local and global widths scale differently. Equivalently, for small lengths, the height-difference correlation function scales as $t^{(\alpha-\alpha_{\text{loc}})/z} = t^{(\alpha-1)/z}$. Since $(\alpha - \alpha_{\text{loc}})/z = \beta - \beta_{\text{loc}} = \beta^*$, β^* is termed as the local anomalous growth exponent describing the degree of anomaly of the system.

These expressions imply that if we plot the curves $G_2(r,t)/r^\alpha$ vs $r/t^{1/2}$ for all growth times, all the curves must collapse into a single one. Moreover, if superroughening is present, the slope of this single curve for small $r/t^{1/2}$ values must be equal to $-(\alpha-1)$. Thus, the collapse of these functions is a verification of the consistency of the analysis.²⁵

In the superrough scaling case, PSD(k,t) has the same scaling behavior as in the FV case. Thus, from the PSD(k,t) plots we should obtain a value of α larger than 1. Also, the PSD(k,t) curves obtained for different growth times should overlap for large k values.

Summarizing, the fingerprints of superrough scaling are different scalings of the local and global interface widths. This fact is clearly shown in the $G_2(r,t)$ function as the curves for different times are shifted upwards as the growth time increases in both cases, which is not observed for the PSD(k,t) curves.

Thus, in this work we address the study of the scaling behavior of AlN films grown by dc reactive sputtering under this theoretical framework. The surface morphology of the films deposited for different times has been analyzed by atomic force microscopy (AFM). The scaling properties of both $G_2(r,t)$ and PSD(k,t) have been studied in order to properly identify the growth mode.

II. EXPERIMENT

AlN films were deposited on (100)-oriented silicon substrates at room temperature in a dc reactive magnetron sputtering system described previously.⁶ The target-substrate distance was 6.5 cm. Sputtering from a high-purity (99.999%) aluminum target was performed at 100-W dc discharge power in an Ar and N₂ working gas mixture. The vacuum pumping system, composed of a turbomolecular pump backed by a mechanical pump, provided a base pressure lower than 10⁻⁶ mbar. The working pressure was $\sim 4 \times 10^{-3}$ mbar when using the selected gas mixture of 29.5-SCCM (standard cubic centimeter per minute) total flow (20% Ar, 80% N₂). These deposition conditions enable to grow stoichiometric AlN films (AlN_x, with x close to 1) at a constant growth rate of 5 nm/min. In order to study the roughness evolution of AlN, a series of films was grown at deposition times ranging from 12 up to 200 min.

Cross sections of the films were analyzed by scanning electron microscopy (SEM) with a Hitachi S-2700 equipment. The samples were also imaged in air by atomic force microscopy (AFM) using a Nanoscope IIIa (Digital Instruments, CA) equipment operating in the tapping mode. Silicon cantilevers with a nominal radius of curvature of 10 nm were employed. Note that, due to the relative hardness of the AlN films (~ 20 GPa), the tapping mode AFM imaging is more reliable than the contact-mode imaging since the tip-sample interaction is considerably lower, leading to less tip damaging and, therefore, less tip convolution effects. AFM images over scanning areas of 500×500 nm² with a resolution of 512×512 pixels were used to extract the calculations shown below.

The crystalline structure of the layers was examined by x-ray diffraction (XRD). The XRD measurements were per-

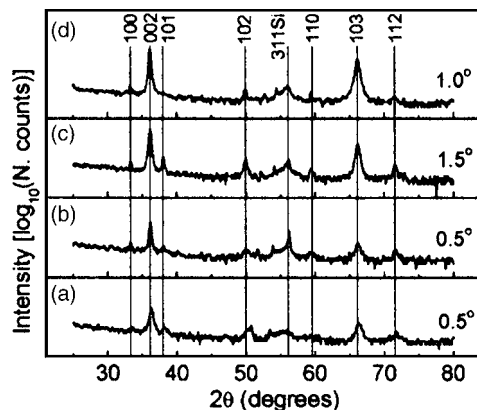


FIG. 1. Grazing incidence XRD patterns for (a) 12-, (b) 36-, (c) 100-, and (d) 200-min-deposited films. The values indicated in the figure are the angles of incidence measured from each sample surface. 002 preferential orientation can be observed for all samples.

formed at Cu $K\alpha$ wavelength on a Siemens D 5000 diffractometer in surface-sensitive grazing incidence (GI) modes at different incidence angles fixed at 0.5°, 1.0°, and 1.5°. The diffraction patterns obtained in all the films did not show any important difference, as in all cases the polycrystalline hexagonal structure of wurtzite-type was observed (File No. 25-1133 of JCPDS-ICDD diffraction database PDF-2). Figure 1 shows the GI diffraction patterns obtained from some samples of the series, where we can observe a c -axis preferred orientation in them. The 002 diffraction is always the strongest one, indicating a preferred orientation of (001)

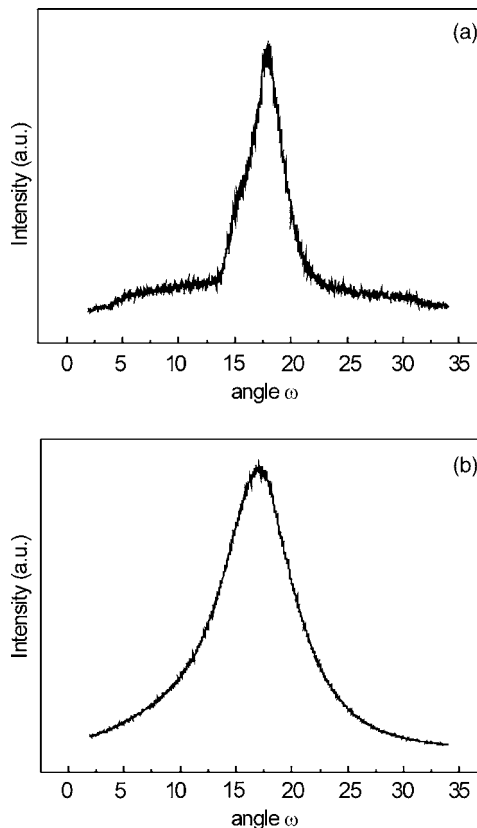


FIG. 2. Rocking curves of the (a) 12- and (b) 200-min AlN films, measured with the detector fixed at the 002 diffraction angle. The angle ω is the incidence angle measured from the sample surface.

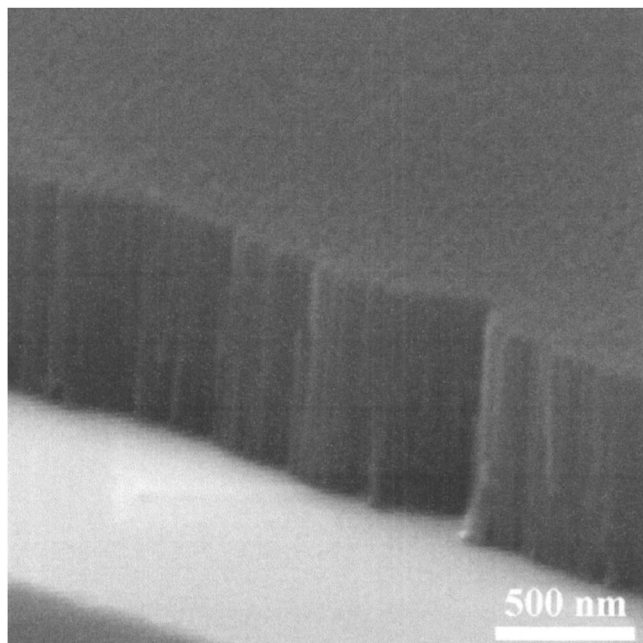


FIG. 3. SEM image of a cross section of an 800-nm-thick AlN film.

planes parallel to the substrate surface with a rather broad angular distribution. It can be observed that the height of this peak increases with the film thickness.

Besides, rocking curves on the 002 diffraction, typical for the texture observed, have also been measured. These analyses of the texture perfection of the films did show differences between the films. Namely, the rocking curves measured on the samples deposited for times longer than 36 min display a simple symmetric bell-like shape [Fig. 2(b)], while the corresponding rocking curves of the films grown for $t < 36$ min are more complex [Fig. 2(a)]. The simple shape indicates a uniformly developed texture over the film volume, while the more complex one suggests the presence of well-textured regions with aligned grains, producing the sharp ridge around the specular position, which are embedded in a rather randomly oriented matrix contributing to the broad baseline. Thus, two different film textures are observed in the layers as the growth time increases. Particularly, in the early stages of the film growth ($t < 36$ min), the polycrystalline films display randomness in the grain orientation, in agreement with other reports.^{26,27} As the growth proceeds, the films developed a (002) preferred orientation in the form of a columnar structure. The column axes are mutually misaligned, as can be seen also in the SEM image of Fig. 3, which explains a rather large width of the bell-like-shaped rocking curves stretching up to the grazing incidence/exit regions.

III. RESULTS

Figure 4 shows the surface morphology of AlN films for increasing deposition times obtained by AFM. These images show clearly both the surface roughening as well as the coarsening of the characteristic lateral length distance, ξ , as the growth time increases. From the AFM data, several morphological functions can be obtained. The most evident is the

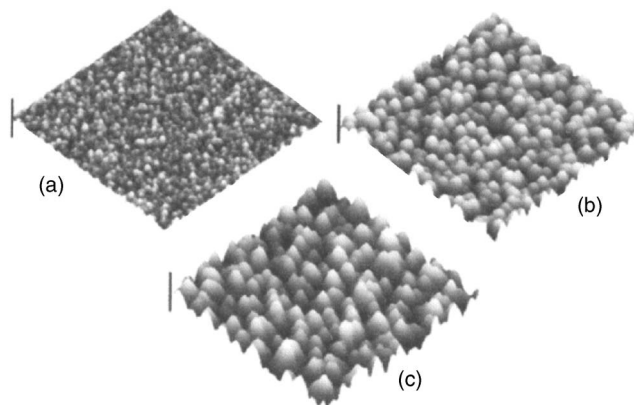


FIG. 4. 500×500 -nm² AFM images of AlN films grown on Si(100) substrates for (a) 12, (b) 60, and (c) 200 min. The vertical bars indicate 50 nm.

dependence of the global width or root-mean-square roughness w with the growth time [Fig. 5(a)]. Two regions can be clearly observed. The first one, for the shorter deposition times, shows an exponential dependence of the surface roughness with time, which is also compatible with a very high β values, $\beta \geq 1$. In contrast, in the second growth regime, for $t > 36$ min, a power-law dependence, $w \propto t^\beta$, with $\beta = 0.37 \pm 0.03$ is found. The exponential dependence observed in the first region implies that the growth is clearly unstable. In the second growth regime, the roughening is appreciably lower as $\beta = 0.37 \pm 0.03$. However, this value is

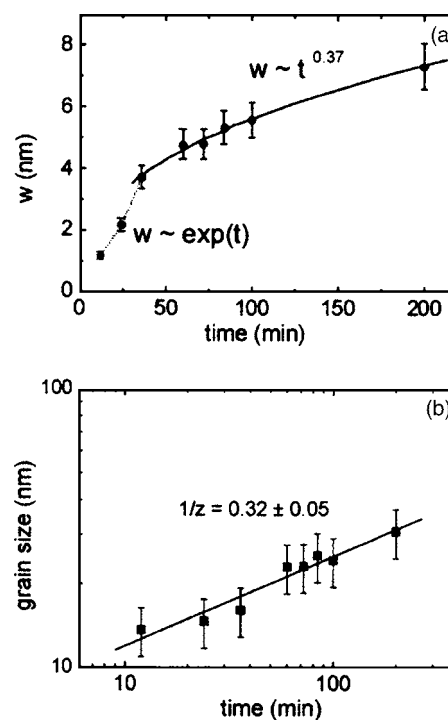


FIG. 5. (a) Plot of the AlN film surface roughness as a function of growth time. Two growth regimes are observed, with a crossover time of 36 min. The first one, for short deposition times, is compatible with an exponential dependence of the surface roughness with growth time, the dotted line indicating the best exponential fit of the data. For the second regime, for $t > 36$ min a power-law dependence, $w \propto t^\beta$, with $\beta = 0.37$ is observed, the dashed line corresponding with the best power-law behavior. (b) Logarithmic plot of the average grain size as a function of growth time. The coarsening exponent ($1/z$) value is indicated.

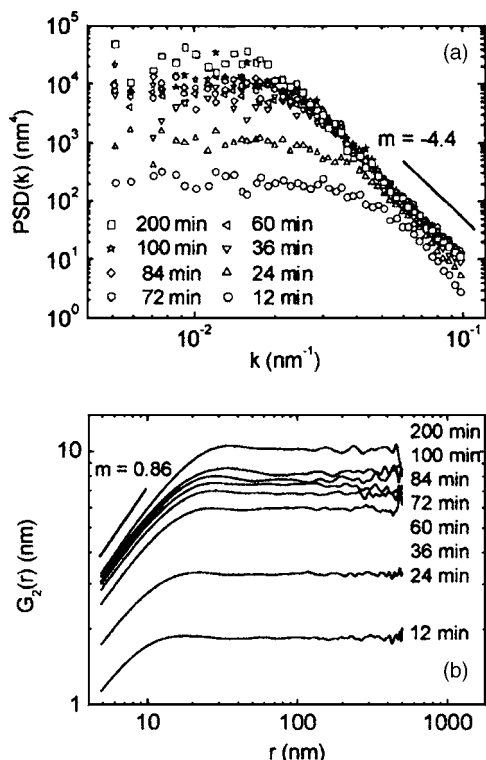


FIG. 6. (a) Logarithmic plot of the PSD functions vs wave number k , corresponding to different growth times. The slope of the PSD curves for large k values is indicated. (b) Logarithmic plot of the $G_2(r, t)$. The slope of the $G_2(r, t)$ curves for small r values is indicated.

higher than those expected for the growth models governed by stabilization mechanisms such as surface diffusion, lateral growth, or surface tension.² Figure 5(b) shows the logarithmic plot for the evolution of ξ obtained directly from the AFM images. In this case, a single coarsening exponent value $1/z = 0.32 \pm 0.05$ (i.e., z close to 3) is found for the whole temporal range in our experiment.

The existence of these two growth regimes has to be confirmed by the analysis of the evolution of the $PSD(k, t)$ and $G_2(r, t)$ functions with the deposition time. The results are displayed in Figs. 6(a) and 6(b), respectively. As can be seen in Fig. 6(a), it is clear that all curves are composed of two regions: (a) for high k values (i.e., small length scales) there is a negative slope, indicating the existence of kinetic roughening for these length scales; (b) for small k values (i.e., large length scales) the curves are almost horizontal (i.e., saturated), indicating the absence of any lateral correlation in the surface roughness at these length scales. From the figure, it is evident that the PSD curves are shifted upwards as the deposition time increases for the first growth regime (i.e., up to 36 min of deposition), while they overlap within the second growth regime. Thus, the temporal evolution of the PSD curves does confirm the existence of two growth regimes, with a crossover close to $t = 36$ min. This fact is also reflected in Fig. 6(b), where the $G_2(r, t)$ functions are plotted for different deposition times. During the whole experiment the $G_2(r, t)$ functions are shifted upwards as the growth time increases. However, this shift is steeper and larger for the samples grown during the first growth regime than for those deposited during the second one.

Thus, we can conclude from these analyses that there are two growth regimes with a crossover time close to 36 min.

A. First growth regime ($t \leq 36$ min)

This regime is characterized by the exponential dependence of the film surface roughness with the increasing deposition time [Fig. 5(a)], also compatible with $\beta \geq 1$, within our temporal resolution. This result implies that the growth is unstable in this deposition time range. Accordingly, both the PSD and $G_2(r, t)$ functions show a vertical shift as the growth time increases. Under these unstable growth conditions, the growth is favored in the vertical rather than lateral (along the substrate plane) direction. Furthermore, in this regime the shift of the $G_2(r, t)$ functions is quite distinct. This behavior implies that local surface slopes increase steeply in this regime.¹⁶ A similar behavior, namely, the existence of anomalous scaling during unstable growth, has been found for a continuum equation describing amorphous thin-film growth by vapor deposition.²⁸

B. Second growth regime ($t \geq 36$ min)

From the data displayed in Fig. 6, we have found that in this growth regime the PSD functions do overlap, whereas $G_2(r, t)$ functions are shifted upwards as the deposition time increases. This behavior is a clear indication that the growth follows the laws of superroughening, which is further confirmed by computing the slope of the PSD curves for large k values. From this slope we obtain a value $\alpha = 1.2 \pm 0.2 > 1$, which supports this interpretation. However, some problems arise when we compute the slope of the $G_2(r, t)$ functions for small r values, since we obtain $\alpha_{loc} = 0.86 \pm 0.04 < 1$. As explained before, α_{loc} should be equal to 1 when superroughening operates. However, we believe that this disagreement lies on the computational limitations of the $G_2(r, t)$ function that make it impossible to obtain the values of α_{loc} close to 1.²⁹⁻³¹ In order to reliably check this limitation we have performed a 2+1 numerical integration of the *linear* molecular-beam epitaxy (MBE) growth equation, which is known to follow a superrough behavior.^{21,23,25} When we evaluated the corresponding $G_2(r, t)$ function we obtained also a value clearly smaller than 1, whereas we obtained the expected values for the other exponents. It has to be stressed that α_{loc} should be exactly equal to 1 in this case.

Taking into account this inherent computational limitation of $G_2(r, t)$, we can then assume that $\alpha_{loc} = 1$. We can summarize our findings as (i) global exponents: $\alpha = 1.2 \pm 0.2$, $\beta = 0.37 \pm 0.03$, and $1/z = 0.32 \pm 0.05$ (note that these values, obtained independently, obey, within the error bars, the scaling relationship $\beta = \alpha/z$); and (ii) local exponents: $\alpha_{loc} = 1$ and $\beta_{loc} = \alpha_{loc}/z = 0.32 \pm 0.01$. These results imply $\beta^* = 0.05 \pm 0.02$, that is, a small, although noticeable, anomaly.

One way to check the validity of our analysis is to try to collapse the $G_2(r, t)$ functions obtained for the different deposition times by plotting the function $G_2(r, t)/r^\alpha$ vs $r/t^{1/z}$ as described in the Introduction, Eq. (7). If the system does not show anomalous scaling, the slope at small abscissas, m_1 , should be equal to 0, as $\alpha = \alpha_{loc}$. However, for our system the excellent collapse (Fig. 7), obtained by using $1/z$

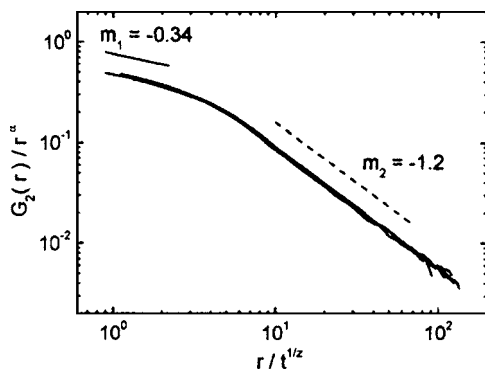


FIG. 7. Collapse of the $G_2(r, t)$ functions for the superrough growth regime using exponents $\alpha=1.2$ and $1/z=0.32$. The straight lines correspond to $u^{-\alpha}$ (dashed) and $u^{-(\alpha-\alpha_{loc})}$ (solid).

$=0.32 \pm 0.05$ and $\alpha=1.2 \pm 0.2$, clearly shows two regions with negative slopes. Accordingly, the slope at large x -axis arguments, m_2 , is equal to -1.2 , which is consistent with α as it should occur within the superrough scaling framework, Eq. (7).²⁴ For small arguments $m_1 = -0.32$, which, within the error bars, correspond to $-(\alpha - \alpha_{loc})$ taking into account that the measured value of α_{loc} is 0.86 ± 0.04 because of the computational limitations of $G_2(r, t)$.

IV. DISCUSSION

Our data indicate that AlN growth has two regimes, the first one, for $t < 36$ min, being unstable and the second one, for $t > 36$ min, displays superrough scaling with a global β values of 0.37 ± 0.03 . However, a single coarsening exponent, $1/z = 0.32 \pm 0.05$, is observed regardless of the deposition time. Both regimes present roughening behaviors that are not explained by any of the models, including stabilization mechanisms such as surface diffusion, evaporation–condensation processes, or lateral growth,² although some approximate evidence can be extracted from generic models. In fact, many of the scaling studies of the films deposited by sputtering share this behavior, as they display β values ranging from 0.4 up to 0.8. These values are mainly found for polycrystalline systems^{17,18,32–35} and also for amorphous silicon.¹⁹ Finally, for sputtered deposition of platinum on glass, with simultaneous substrate rotation, it was found that the growth dynamics is governed by linear diffusion.¹⁶

In order to obtain a better insight of the possible physical mechanisms determining the film growth dynamics the observed (002) preferred orientation of the AlN films could be an interesting issue. Recently, Kajikawa *et al.* have studied the mechanisms involved in the preferred orientation of AlN films grown by sputtering deposition,²⁷ namely, sticking anisotropy and surface diffusion. We must consider also shadowing as a crucial mechanism in our system. Let us analyze each mechanism independently.

As we have reported above, our system displays a single coarsening exponent $1/z = 0.32 \pm 0.05$ regardless of the deposition time, which, within the error bars, is consistent with that due to shadowing effects.³⁶ This result suggests that shadowing is operating during the film growth in our system. To check the validity of this assumption, we remind that our AlN sputtering deposition is reactive; the Al species sput-

tered from the target are deposited on the substrate, which is at room temperature, and the N-active species present in the plasma impinge on the growing film with a sticking coefficient close to 1.³⁷ Under our pressure-deposition conditions, the system is below the thermalization threshold³⁸ and the average mean free path of the Al species, λ , is ≈ 5 cm, which is of the order of the target–substrate distance. This implies that Al and N species do not react within the plasma but, rather, at the growing film surface. Thus, we can assume, in a first approximation, that the impinging particles are Al and N species following ballistic trajectories. Furthermore, it is known that the flux of sputtered target particles follows a cosine distribution in sputtering processes.³⁹ These facts indicate that shadowing effects could play an important role in the film growth dynamics as other authors have already suggested.^{16,18,19} Shadowing effects imply a scenario in which one type of region, usually those located at higher surface positions (“bumps”), grows faster at the expense of others (“valleys”), which is known to lead to unstable growth morphologies with large β values.⁴⁰ Models of shadowing in 2+1 dimensions predict $1/z = 1/3$ and $\beta = 1$.⁴⁰ However, recently, Yu and Amar have studied theoretically the dynamic scaling of ballistic deposition with shadowing on unidimensional substrates.³⁹ In this work, they consider explicitly two conditions for the angular distribution of the impinging particles: uniform angular distribution and cosine distribution. They found that, in fact, the former condition, which is the standard one used in the models of shadowing, corresponds to an anisotropic flux of particles on the growing surface. In contrast, the latter one, which is close to that taking place in sputtering deposition, implies an isotropic flux. Moreover, they reported that, for a cosine distribution, the β value was smaller than that obtained for the anisotropic flux, that was close to 1. Thus, shadowing effects could lead to still high β values for sputtering deposition, but clearly smaller than the value $\beta \approx 1$ predicted by many models. It should be recalled that for our system conditions, where λ is close to the target–substrate distance, the impinging particles follow ballistic trajectories as in the model of Yu and Amar. Besides, a vertical shift with increasing deposition time was obtained for the $G_2(r)$ functions in this unidimensional system,³⁹ similarly as in ours. Unfortunately, this study was performed only for unidimensional substrates, whereas realistic substrates are two-dimensional, which prevents direct comparison of the experimental exponents with the theoretical ones.² However, the trend of smaller β values for a cosine distribution should be obeyed also on two-dimensional substrates. Moreover, the fact that many of the reported β values for sputtering systems lie in the 0.4–0.6 range supports this interpretation. Besides, in some of these systems, the $G_2(r, t)$ function evaluated from scanning probe microscopy (SPM) data shifts vertically as the growth time increases, similarly as in our system, although the data were not analyzed under the framework of anomalous scaling.^{19,33} Finally, it is worth to remark that for the only sputtering system in which a low β value was obtained,¹⁶ shadowing effects were intentionally eliminated by rotating the sample during the deposition process.

Surface diffusion mechanism could be predominant in

our system. However, the deposition process takes place at room temperature and the surface temperature during the growth process does not exceed 350 K, even for the longest deposition times. In principle, this fact implies that important surface diffusion relaxation processes should not be expected. Moreover, if surface diffusion processes were predominant, the corresponding observed scaling behavior should be compatible with that predicted by the MBE model, which is not the case.²

Although our system shows two different roughening behaviors, a rapid and unstable roughening for short deposition times, and $\beta=0.37\pm 0.03$ for $t>36$ min, it possesses a single coarsening exponent. The existence of these two regimes correlates with the existence of two types of polycrystalline textures depending on the film-growth time (Fig. 2). Thus, we can understand the single coarsening exponent from the shadowing considerations done above, but both shadowing and polycrystallinity effects may determine the growth exponent. Whereas shadowing effects should be present to the same extent regardless of the film thickness, the magnitude of the latter ones could change due to the observed film texture evolution. Namely, we have to assume that sticking processes are closely related to the preferred orientation of the films, which results in the sticking anisotropy, i.e., the fact that the impinging particles experience different sticking probabilities on different crystalline planes.²⁷ In our system this effect should likely appear during the first growth regime since well-aligned and textured grains are embedded into a randomly oriented matrix. Under this assumption, these regions having a higher sticking probability should grow faster than the other types of regions. This scenario, combined with shadowing, may lead to a sort of competitive growth, leading to the observed growth instability with a high β value ($\beta\sim 1$). Such a result is compatible with the observed steep increment of the local surface slope. In the second growth regime, the film reaches a homogeneous and well-defined texture, implying that the sticking probability is similar across the whole surface. Under these conditions, the growth is 'rather' stabilized, leading to smaller β values.

V. CONCLUSIONS

We have found that deposition of AlN films on silicon substrates by dc reactive sputtering shows two growth regimes. The first one occurs during the first 36 min of deposition, being an unstable transient characterized by an intense roughening. In contrast, in the second regime, for deposition times higher than 36 min, a relative stabilization of the surface is achieved since $\beta=0.37\pm 0.03$, although this value is still higher than those predicted by available models with stabilized surface. A superrough scaling behavior is found for this regime with the following exponent values: (i) Global exponents: $\alpha=1.2\pm 0.2$, $\beta=0.37\pm 0.03$, and $1/z=0.32\pm 0.05$; (ii) local exponents: $\alpha_{loc}=1$ and $\beta_{loc}=\alpha_{loc}/z=0.32\pm 0.01$. We have also found a correlation between the film texture and the AlN growth mode. In the first regime, the films contain two types of textured regions, well textured and randomly ordered, respectively. These regions have likely different sticking probabilities for the impinging particles. Thus, in

this first growth regime, a competitive growth takes place and leads to the observed unstable growth. In the second growth regime, the film being homogeneous and well textured, this sticking anisotropy vanishing. Under this scenario, the growth is dominated by shadowing effects induced by the ballistic deposition of the impinging particles having a cosine angular distribution (i.e., an isotropic flux at the growing surface) combined with the preferential sticking due to surface anisotropy. This type of deposition leads to growth with β values clearly smaller than those usually predicted by the shadowing models (i.e., $\beta\approx 1$), in qualitative agreement with our results and with those reported for other sputtering systems.

ACKNOWLEDGMENTS

Financial support from Spanish MCyT: Projects No. MAT 2002-04037-C03-03 and BFM 2003-07749-C05-01, BFM 2003-07749-C05-02, and BFM 2003-07749-C05-05, European Community: Project No. G5RD-CT-2000-00333, Slovak governmental Project No. 2003-SO 51/03R0600/01, and Slovak Grant Agency for Science VEGA, Project No. 2/3149/23, are acknowledged.

- ¹J. Krim and G. Palasantzas, *Int. J. Mod. Phys. B* **9**, 599 (1995).
- ²A.-L. Barabási and H. E. Stanley, *Fractal Concepts in Surface Growth* (Cambridge University Press, Cambridge, 1995).
- ³P. Meakin, *Fractals, Scaling and Growth Far from Equilibrium* (Cambridge University Press, Cambridge, 1998).
- ⁴R. Cuerno and L. Vázquez, in *Advances in Condensed Matter and Statistical Physics*, edited by E. Korutcheva and R. Cuerno (Nova Science, NY, 2004).
- ⁵F. Ojeda, R. Cuerno, R. Salvarezza, and L. Vázquez, *Phys. Rev. Lett.* **84**, 3125 (2000); F. Ojeda, R. Cuerno, R. Salvarezza, F. Agulló-Rueda, and L. Vázquez, *Phys. Rev. B* **67**, 245416 (2003).
- ⁶M. A. Auger, R. Gago, M. Fernández, O. Sánchez, and J. M. Albella, *Surf. Coat. Technol.* **157**, 26 (2002).
- ⁷E. Vacandio, Y. Massiani, P. Gergaud, and O. Thomas, *Thin Solid Films* **359**, 221 (2000).
- ⁸M. B. Assour, O. Elmazria, L. Le Brizoual, and P. Alnot, *Diamond Relat. Mater.* **11**, 413 (2002).
- ⁹R. Y. Kruspitskaya, *J. Appl. Phys.* **84**, 2862 (1998).
- ¹⁰M. Mosca, J. L. Reverchon, F. Omnès, and J. Y. Duboz, *J. Appl. Phys.* **95**, 4367 (2004).
- ¹¹J. N. Kuznia, M. A. Khan, D. T. Olson, R. Kaplan, and J. Freitas, *J. Appl. Phys.* **73**, 4700 (1993).
- ¹²D. G. Zhao, J. J. Zhu, Z. S. Liu, S. M. Zhang, and H. Yang, *Appl. Phys. Lett.* **85**, 1499 (2004).
- ¹³M. B. Assour, O. Elmazria, M. Elhakiki, and P. Alnot, *J. Vac. Sci. Technol. B* **22**, 1717 (2004).
- ¹⁴Q. Guo, M. Nishio, H. Ogawa, and A. Yoshida, *Phys. Rev. B* **55**, R15987 (1997).
- ¹⁵H. Harris, N. Biswas, H. Temkin, S. Gangopadhyay, and M. Strathman, *J. Appl. Phys.* **90**, 5825 (2001).
- ¹⁶J. H. Jeffries, J. K. Zuo, and M. M. Craig, *Phys. Rev. Lett.* **76**, 4931 (1996).
- ¹⁷H. You, R. P. Chiarello, H. K. Kim, and K. G. Vandervoort, *Phys. Rev. Lett.* **70**, 2900 (1993).
- ¹⁸M. Saitou, A. Makabe, and T. Tomoyose, *Europhys. Lett.* **52**, 185 (2000).
- ¹⁹T. Karabacak, Y. P. Zhao, G. C. Wang, and T. M. Lu, *Phys. Rev. B* **64**, 085323 (2001).
- ²⁰F. Family and T. Vicsek, *J. Phys. A* **18**, L75 (1985).
- ²¹S. Das Sarma, S. V. Ghaisas, and J. M. Kim, *Phys. Rev. E* **49**, 122 (1994).
- ²²S. Huo and W. Schwarzacher, *Phys. Rev. Lett.* **86**, 256 (2001).
- ²³J. M. López, M. A. Rodríguez, and R. Cuerno, *Phys. Rev. E* **56**, 3993 (1997).
- ²⁴J. J. Ramasco, J. M. López, and M. A. Rodríguez, *Phys. Rev. Lett.* **84**, 2199 (2000).
- ²⁵J. M. López, M. A. Rodríguez, and R. Cuerno, *Physica A* **246**, 329 (1997).

- ²⁶Y.-J. Yong, J.-Y. Lee, H. S. Kim, and J. Y. Lee, *Appl. Phys. Lett.* **71**, 1489 (1997).
- ²⁷Y. Kajikawa, S. Noda, and H. Komiyama, *J. Vac. Sci. Technol. A* **21**, 1943 (2003).
- ²⁸M. Raible, S. J. Linz, and P. Hänggi, *Phys. Rev. E* **64**, 031506 (2001).
- ²⁹M. Siegert, *Phys. Rev. E* **53**, 3209 (1996).
- ³⁰R. Kant, *Phys. Rev. E* **53**, 5749 (1996).
- ³¹J. Schmittbuhl, J. P. Villote, and S. Roux, *Phys. Rev. E* **51**, 131 (1995).
- ³²R. M. Öksüzoglu, A. Elmali, T. E. Weirich, H. Fuess, and H. Hahn, *J. Phys.: Condens. Matter* **12**, 9237 (2000).
- ³³N.-E. Lee, D. J. Cahill, and J. E. Greene, *Phys. Rev. B* **53**, 7876 (1996).
- ³⁴J. Wang, G. Li, P. Yang, M. Cui, X. Jiang, B. Dong, and H. Liu, *Europhys. Lett.* **42**, 283 (1998).
- ³⁵J.-P. Schlomka, M. Tolan, and W. Press, *Appl. Phys. Lett.* **76**, 2005 (2000).
- ³⁶J. H. Yao and H. Guo, *Phys. Rev. E* **47**, 1007 (1993).
- ³⁷D. L. Smith, A. S. Alimonda, and F. J. von Preissig, *J. Vac. Sci. Technol. B* **8**, 551 (1990).
- ³⁸T. Salditt *et al.*, *Phys. Rev. B* **54**, 5860 (1996).
- ³⁹J. Yu and J. Amar, *Phys. Rev. E* **66**, 021603 (2002).
- ⁴⁰D. Le Bellac, G. A. Niklasson, and C. G. Granqvist, *Europhys. Lett.* **32**, 155 (1995).